Simulating ice nucleation, one molecule at a time, with the 'DFT microscope'†

Angelos Michaelides[abc]

Received 15th November 2006, Accepted 1st February 2007
First published as an Advance Article on the web 11th April 2007
DOI: 10.1039/b616689j

Few physical processes are as ubiquitous as the nucleation of water into ice. However, ice nucleation and, in particular, heterogeneously catalyzed nucleation remains poorly understood at the atomic level. Here, we report an initial series of density functional theory (DFT) calculations aimed at putting our understanding of ice nucleation and water clustering at metallic surfaces on a firmer footing. Taking a prototype hydrophobic metal surface, Cu(111), for which scanning tunneling microscopy measurements of water clustering have recently been performed, possible structures of adsorbed clusters comprised of 2–6 H_2O molecules have been computed. How the water clusters in this size regime differ from those in the gas phase is discussed, as is the nature of their interaction with the substrate.

1. Introduction

H_2O–metal interactions are important in a wide variety of phenomena in materials science, catalysis, corrosion, electrochemistry, and so on. H_2O–metal interfaces also provide fertile ground for understanding basic physical processes such as ice nucleation and water clustering. In this respect a wide variety of surface science style studies have been performed, focussing on understanding the structures and properties of thin ice films and water overlayers that form on well-defined single-crystal metal surfaces under ultra-high vacuum (UHV) conditions. By now such overlayer systems have been interrogated with almost every available experimental surface science probe as well as a variety of theoretical approaches.[1–3]

Many of the recent studies in this area have focussed on determining the nature and structures of the first wetting layer of H_2O–ice that may form. Due to the competing influences of H_2O–metal bonding and H_2O–H_2O epitaxial mismatch between the overlayer and the substrate a wide variety of extended overlayer structures have been proposed, such as 2D ice-like overlayers[4–9] quasi-2D overlayers,[10] 1D chains,[11] and mixed H_2O–OH overlayers.[12–19] Several of these overlayer systems have been examined with a range of complementary experimental and theoretical techniques such as low-energy electron diffraction (LEED), vibrational spectroscopies, photoemission, and density functional theory (DFT) leading to a clear atomic-scale characterisation of their structures.

Much less is known, however, about the structures of small H_2O clusters that form prior to the creation of the extended overlayers; dimers, trimers, tetramers, *etc.* Although on a few metal surfaces some of the clusters have been reported in infrared

[a] *London Centre for Nanotechnology, University College London, London, UK WC1E 6BT*
[b] *Department of Chemistry, University College London, London, UK WC1E 6BT*
[c] *Fritz-Haber-Institut der Max-Planck-Gesellschaft, Faradayweg 4-6, 14195, Berlin, Germany*

† The HTML version of this article has been enhanced with colour images.

reflection absorption (IRAS) spectroscopy[20–22] and scanning tunnelling microscopy (STM)[3,23–25] studies their internal structure or registry with the substrate remains, in every case, unclear. Moreover, it is not known how the structures and relative energies of the adsorbed clusters differ from the equivalent clusters in the gas phase. It is in this regard that first principles electronic structure theories can make valuable contributions. And, indeed, adsorbed H_2O monomers and small H_2O clusters have recently been computed with DFT on a number of close-packed metal surfaces providing predictions as to what structures may form as well as insight and understanding as to why particular structures are favoured over others.[26–34]

The study reported here is in a similar spirit to the previous DFT studies cited above. However, here we examine, for the first time, adsorbed clusters right up to the H_2O hexamer; dimers, trimers, tetramers, pentamers, and hexamers have all been computed. In addition we examine how the structures and stability of these small H_2O clusters differ from those in the gas phase, thus shedding light on the 'catalytic' role of the Cu(111) substrate in H_2O cluster formation. We have chosen Cu(111) for this work mainly because recent low temperature STM experiments of H_2O and D_2O clustering have been reported on this surface.[35] In addition, Cu(111) is of interest because it is a substrate upon which H_2O does not normally dissociate and is an hexagaonl surface which can, in principle, support an adsorbed H_2O–ice bilayer with a lattice mismatch of $<2\%$.[1,36]

The plan for the remainder of this paper is the following. Details of our first principles total energy calculations are outlined below. Following this structures and energetics for the adsorbed H_2O clusters are presented (section 3). In section 4 we briefly discuss our results, paying particular attention to the electronic structures of adsorbed H_2O dimers and hexamers. In section 5 we close by drawing some conclusions.

2. Approach and computational details

The majority of the calculations reported here have been performed within the DFT framework as implemented in the CASTEP code.[37] The electron–ion interactions were treated with Vanderbilt ultrasoft pseudopotentials,[38] which were expanded within a plane-wave basis set up to a cut-off energy of 400 eV. Electron exchange and correlation effects were described by the Perdew Burke Ernzerhof (PBE)[39] generalized gradient approximation (GGA).

The Cu(111) surface was modelled by a periodic array of Cu slabs, separated by a vacuum region in excess of 12 Å. The majority of the adsorption calculations were performed in $p(4 \times 4)$ or $p(5 \times 5)$ unit cells. Such large cells were required in order to minimize the interaction between water clusters in adjacent unit cells. Because of the relatively large unit cells employed and the desire to explore a wide variety of structures for each cluster, thin 3 layer Cu slabs were used throughout. The significance of this apparent compromise in accuracy was, however, carefully checked with test calculations for adsorbed water clusters on slabs of up to 9 layers thickness. The main results of these tests are shown in Table 1, where it can be seen that the absolute adsorption energies obtained on the thicker slabs deviated by <10 meV per H_2O and bond distances deviated by <0.1 Å. Monkhorst–Pack $\boldsymbol{k}$-point meshes with the equivalent of at least $8 \times 8 \times 1$ sampling within the surface Brillouin zone of a $p(1 \times 1)$ unit cell were used throughout.[40]

In all optimizations the bottom two Cu layers were fixed at their *ab initio* bulk truncated positions (3.647 Å (expt 3.615 Å[41])) and the remaining atoms were allowed to fully relax. For each cluster a large number of trial structures were optimized; as many as 30 trial structures for the pentamers and hexamers. In addition, the occasional simulated annealing *ab initio* molecular dynamics simulation was performed. However, we caution that configurational space becomes so large for systems with >2–3 adsorbed and interacting H_2O molecules that we can in no way guarantee that the structures identified are the global minimum energy

Table 1 Selected results of the layer and ***k***-point sampling convergence tests for H_2O monomer and H_2O cluster (dimer and hexamer) adsorption on Cu(111)

Adsorbate	Layers	***k*** mesh[a]	E_{ads} (meV/H_2O)	Cu–O[b] (Å)	O–O[b] (Å)
Monomer [$p(2 \times 2)$ cell]	3	$8 \times 8 \times 1$	151	2.345	—
	3	$12 \times 12 \times 1$	146	2.370	—
	3	$24 \times 24 \times 1$	145	2.357	—
	9	$8 \times 8 \times 1$	157	2.347	—
Dimer [$p(3 \times 3)$ cell]	3	$12 \times 12 \times 1$	321	2.202/3.032	2.740
	3	$18 \times 18 \times 1$	327	2.199/3.026	2.740
	9	$12 \times 12 \times 1$	332	2.152/2.934	2.716
Hexamer [$p(4 \times 4)$ cell]	3	$8 \times 8 \times 1$	440	2.772	2.697
	3	$16 \times 16 \times 1$	435	2.771	2.697
	9	$8 \times 8 \times 1$	444	2.802	2.696

[a] $p(1 \times 1)$ equivalent sampling. [b] Average values are given for the hexamer.

structures. At best the structures identified serve merely as plausible candidates for the lowest energy adsorption structures of H_2O clusters that may form on Cu(111).

Adsorption energies (E_{ads}) per H_2O molecule are calculated from,

$$E_{ads} = nE_{H_2O} + E_{Cu} - E_{nH_2O/Cu}, \quad (1)$$

where E_{H_2O}, E_{Cu} and $E_{nH_2O/Cu}$ are the total energies of an *isolated* H_2O molecule, the clean Cu(111) surface, and the nH_2O/Cu(111) adsorption system, respectively. In this definition positive adsorption energies correspond to an exothermic adsorption process. The reference energy of the isolated gas phase H_2O molecule is calculated by placing it in a 20 $Å^3$ cell. Calculations of gas phase H_2O clusters have also been performed within the same 20 $Å^3$ cell, for which their gas phase binding energy (E_{bind}) is defined as,

$$E_{bind} = nE_{H_2O} - E_{nH_2O}, \quad (2)$$

where E_{nH_2O} is the total energy of the nH_2O gas phase cluster.

3. Results

We now consider the structures and energies of the low energy water clusters predicted by DFT, which represents the main body of results of this study.

3.1 H_2O monomer adsorption

The most stable structure for the H_2O monomer on Cu(111) is displayed in Fig. 1(a) and (b). From Fig. 1(a) it can be seen that H_2O adsorbs preferentially at an atop site and from the side view in Fig. 1(b) it can be seen that the molecular plane lies almost parallel to the surface. This structure has been reported before as the most stable one according to DFT for water adsorbed on Cu(111) and several other close-packed transition metal surfaces.[26] We show it again here simply because it is important to know how a single water adsorbs on Cu(111) in order to understand the structures of the adsorbed clusters that we come to next. The Cu–O bond length is 2.35 Å and the adsorption energy is 0.15 eV per H_2O. The internal structure of the H_2O molecule deforms little upon adsorption: the HOH angle is 1° less that its computed gas phase value of 104.6° and the OH bond lengths are essentially unchanged from their computed gas phase value of 0.98 Å. Indeed also in the H_2O clusters we do not observe any significant changes of the internal structure of the H_2O molecules and thus will not discuss this issue further.

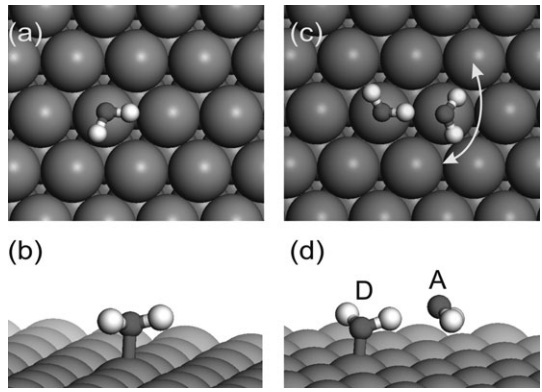

Fig. 1 Top and side views of the lowest energy adsorbed H_2O monomer and H_2O dimer structures identified. In (d) the H_2O molecule which donates (accepts) the H bond is labelled D (A), and in (c) the arrow is to illustrate that rotation of the acceptor H_2O in a plane about the surface normal is facile.

3.2 H_2O dimer adsorption

The most stable adsorbed H_2O dimer structure identified is displayed in Fig. 1(c) and (d). The adsorption energy of this dimer (relative to two isolated H_2O molecules as defined in eqn (1)) is 0.32 eV per H_2O. In this structure both H_2O molecules adsorb above atop sites with the H_2O molecule that donates the H bond (H bond donor, D) noticeably closer to the surface than the H_2O molecule that accepts the H bond (H bond acceptor, A). Specifically the shortest Cu–O bond lengths for the donating and accepting H_2O molecules are 2.20 and 3.00 Å, respectively. The O–O distance in this configuration is 2.74 Å. As was found previously on Pd(111)[28] we see here on Cu(111) that there is essentially free rotation of the high-lying acceptor H_2O about a plane normal to the surface, *i.e.*, the H bond acceptor is not constrained to remain above the precise atop site. For example, rotating the dimer so that the acceptor is located over a bridge site (with the donor still at the atop site) costs a negligible 2 meV.

The lowest energy dimer structure reported here is similar to the structures previously reported from DFT for dimers on Pt(111)[29] and Pd(111).[28] It was also reported in the previous studies that the H_2O donor interacts more strongly with the substrate than the H_2O acceptor. We provide a general explanation for these observations below.

3.3 H_2O trimer adsorption

Two low energy trimer structures of essentially identical adsorption energy have been identified. These are labelled (a) and (b) in Fig. 2, and are displayed along with a third adsorbed trimer to be discussed in a moment. Also shown in Fig. 2 are the relative energies and structures of all three of these trimers in the gas phase. The two low energy adsorption structures are similar to each other in as much as they are bent structures with only two H bonds connecting the three H_2O molecules. They differ, however, in that structure (b) has one H_2O which donates two H bonds whereas structure (a) does not. The adsorption energy for both trimers is 0.37 eV per H_2O.

It is interesting to see that the two bent adsorbed trimers identified here are not the lowest energy isomers for H_2O trimers in the gas phase. Instead this is a cyclic structure with three H bonds between the three H_2O molecules; each H_2O donates and accepts a single H bond, as can be seen from the upper part of Fig. 2(c).

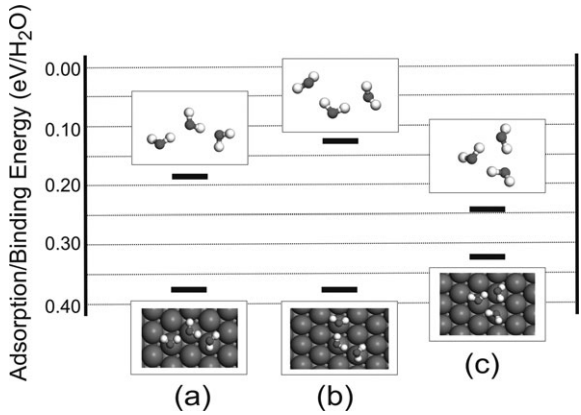

Fig. 2 Relative energies and structures of three gas phase and adsorbed H_2O trimers. Adsorption energies and binding energies are relative to isolated gas phase H_2O molecules as defined in eqn (1) and (2), respectively.

However, from the lower part of Fig. 2(c), it can be seen that when adsorbed the cyclic structure is $\sim$0.05 eV per H_2O less stable than structures (a) and (b). Thus it is clear from structures (a), (b), and (c) that the surface has a significant effect on the relative energies of these isomers, favouring those with only two H bonds. Essentially then the current calculations indicate that one H bond in the trimer breaks upon adsorption.

3.4 H_2O tetramer adsorption

The lowest energy structure identified for the H_2O tetramer is displayed in Fig. 3(a) and (b). This structure resembles one of the low energy trimers (trimer b) but with a fourth H_2O added as a H bond donor to the central H_2O. The binding energy of this cluster is 0.41 eV per H_2O. Again the adsorbed structure differs significantly from the lowest energy gas phase isomer which is, like the trimer, a cyclic structure and is comprised of four H bonds. The O–O distances in the adsorbed structure range from 2.66 to 2.75 Å and the Cu–O distances from 2.20 to 3.10 Å.

3.5 H_2O pentamer adsorption

The most stable H_2O pentamer identified is displayed in Fig. 3(c) and (d). In this structure each H_2O acts as a single H bond donor and a single H bond acceptor,

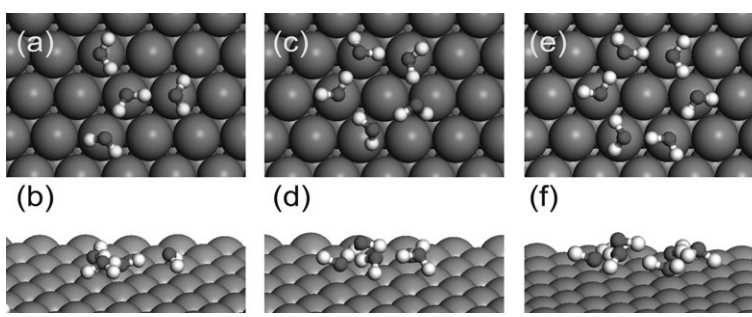

Fig. 3 Top and side views of the lowest energy structures identified for an adsorbed H_2O tetramer ((a)–(b)), pentamer ((c)–(d)), and hexamer ((e)–(f)) on Cu(111).

rather similar to the low energy structure of the gas phase pentamer. Three of the H_2O molecules are located over atop sites, whereas the two others are closest to threefold sites. There is a considerable buckling in the heights of the H_2O molecules above the surface; a 0.8 Å difference between the lowest and highest H_2O molecules. The O–O distances in the adsorbed structure range from 2.60 to 2.80 Å and its adsorption energy is 0.44 eV per H_2O.

3.6 H_2O hexamer adsorption

The most stable hexamer identified is the one shown in Fig. 3(e) and (f). It is a cyclic hexamer with a binding energy of 0.44 eV per H_2O. The symmetry and registry of this cyclic hexamer with the substrate appears to be consistent with recent STM experiments in which it was observed.[35] From the top view of the hexamer in Fig. 3(e) it is clear that all six H_2O molecules are located approximately above substrate atop sites and act as single H bond donors and single H bond acceptors. From the side view in Fig. 3(f) it can further be seen that this structure is significantly buckled with the H_2O molecules residing at two distinct heights above the surface: the vertical displacement between adjacent H_2O molecules is $\sim$0.76 Å. Further, and unlike in the gas phase, the six nearest neighbour O–O distances are not equal in the adsorbed hexamer. Instead they alternate between two characteristic values: 2.76 and 2.63 Å. This symmetry-breaking dimerization is reminiscent of the alternating single and double C–C bonds in the Kekulé model of benzene.

Previous DFT reports of an isolated cyclic hexamer on Ru(0001)[30] and a cyclic hexamer as part of a quasi-2D water overlayer on Pd(111)[10] did not predict the buckled structure identified here. Instead a planar cyclic hexamer with all molecules at the same height was found. Here, on Cu(111), our PBE calculations indicate that the planar hexamer is $\sim$0.12 eV per H_2O less stable than the buckled one. Since it is not inconceivable that this difference is a result of our chosen computational set-up or exchange–correlation functional, we performed a series of tests in order to assess the reliability of this result. Specifically we compared the energy difference between the low energy buckled hexamer identified here and a hypothetical planar cyclic hexamer on: (i) a Cu(111) slab with the RPBE[42] functional; (ii) a close-packed Cu_{10} cluster with the PBE functional, the hybrid DFT PBE0[43] functional, and with Møller–Plesset perturbation theory to second order (MP2).[44] The results of these test calculations are listed in Table 2, with the conclusion of all of them being essentially the same: there is a considerable energetic preference ($>$0.1 eV per H_2O) for buckling on this surface.

Table 2 Selected results of the test calculations of the energy difference, ΔE (meV per H_2O), between the buckled and planar cyclic H_2O hexamers on Cu(111). A positive ΔE indicates that the buckled hexamer is more stable than the planar one, which is always the case

Approach	ΔE (meV/H_2O)
Cu(111) PBE	122[a]
Cu(111) RPBE	178[a]
Cu_{10} cluster PBE	170[b], 175[c]
Cu_{10} cluster PBE0	170[b], 173[c]
Cu_{10} cluster MP2	194[b], 186[d]

[a] Pseudopotential plus plane-wave approach with CASTEP as described in Section II. [b] All-electron Gaussian03 calculation with a 6-311+G(2df,pd) basis set. [c] All-electron Gaussian03 calculation with a 6-311++G(3df,3pd) basis set. [d] All-electron Gaussian03 calculation with a 6-311++G(2df,pd) basis set.

4. Discussion

Let's now briefly investigate some details of the results presented above. First we consider the relative stability of the clusters identified and then several aspects of their electronic structures.

4.1 Relative energies of adsorbed and gas phase clusters

To begin, we compare the stability of the H_2O clusters when adsorbed to when they are in their equilibrium gas phase configurations. We show this in Fig. 4, where the adsorption (binding) energies of adsorbed (gas phase) H_2O clusters ranging from 2–9 H_2O molecules are plotted. The structures of the larger 7–9 molecule gas phase clusters are based on the Hartree–Fock structures reported by Maheshwary *et al.*[45] Here we have simply re-optimized these gas phase structures within the current DFT-PBE set-up. The structures of the 7–9 molecule adsorbed clusters are those recently identified in a combined STM and DFT study of H_2O on Cu(111).[35]

From Fig. 4 it can be seen that in the entire regime examined the adsorbed clusters are more stable than the gas phase ones. It is clear, however, that as the clusters grow in size the energy difference between the adsorbed and gas phase clusters decreases. The increased stability of the adsorbed clusters is obviously because of their binding with the substrate. However, it is interesting to note that the adsorbed clusters remain more stable than their gas phase counterparts even for those clusters which have fewer H bonds when adsorbed. For example the H_2O trimer and tetramer have one less H bond when adsorbed as compared to in the gas phase. And for the larger clusters with 7–9 H_2O molecules several more H bonds are broken.

Also clear from Fig. 4 is that the adsorption energy of the adsorbed clusters gradually decreases until around the pentamer and then seems to level off for the larger clusters. The adsorption energies for the clusters with 5, 6, 7, 8, and 9 molecules are 0.44, 0.44, 0.45, and 0.44 eV per H_2O, respectively. The limiting value of the adsorption energy is at $\sim$0.44 eV per H_2O similar to the adsorption energy reported for a hypothetical 2D ice-like bilayer on Cu(111).[36]

4.2 Electronic structures

Next we briefly consider the nature of the binding between some of the clusters and the Cu(111) substrate. In particular we focus on trying to understand the buckled structure of the H_2O dimer and H_2O hexamer.

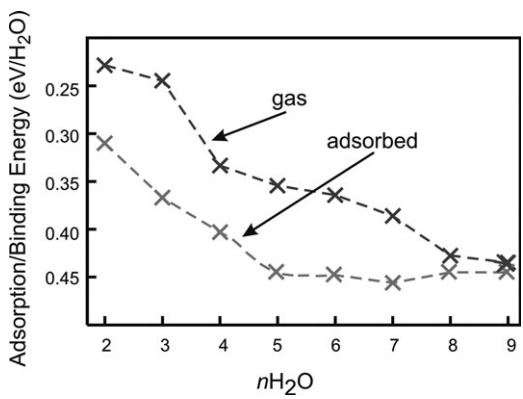

Fig. 4 Plot of the adsorption energies and binding energies for adsorbed nH_2O (n = 2–9) clusters on Cu(111) and for gas phase nH_2O (n = 2–9) clusters. The structures of the 7–9 H_2O molecule gas phase and adsorbed clusters are taken from ref. 45 and ref. 35, respectively. The dashed lines are merely guides to the eye.

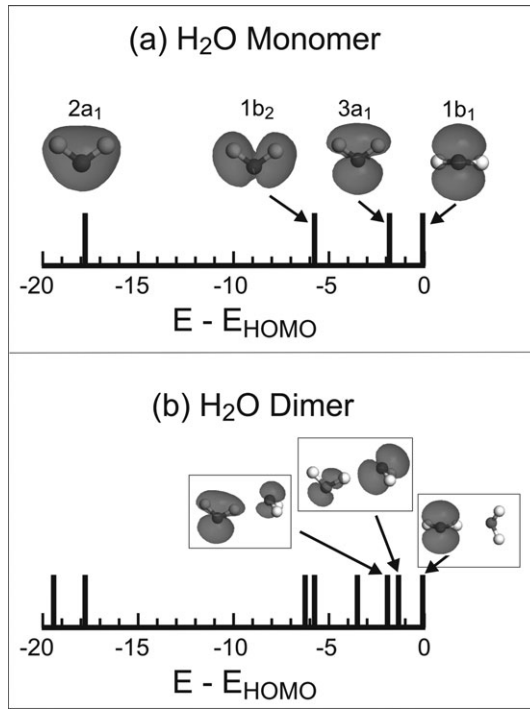

Fig. 5 DFT computed energy level diagrams and selected Kohn–Sham orbitals for the highest occupied orbitals of an isolated (gas phase) H_2O monomer (a) and an isolated (gas phase) H_2O dimer (b). The energy of the highest occupied molecular orbital (E_{HOMO}) is set to zero eV in each system.

A consideration of how the H_2O monomer interacts with the Cu(111) substrate provides a basis for understanding the clusters and so we recall the four highest energy occupied molecular orbitals of an isolated gas phase H_2O (Fig. 5). In order of increasing energy these are labelled, according to C_{2v} symmetry, $2a_1$, $1b_2$, $3a_1$ and $1b_1$. The highest occupied molecular orbital (HOMO) of H_2O is the $1b_1$ orbital. Previous studies have shown that the interaction of the H_2O monomer with close-packed transition metal surfaces is mediated mainly through the $1b_1$ orbital.[17,33] Indeed this is what we find here again for Cu(111). We demonstrate this in Fig. 6(a) with the electron density difference plot for a H_2O monomer on Cu(111). The electron density difference ($\Delta\rho$) is defined here as

$$\Delta\rho = \rho_{n\mathrm{H_2O/Cu}} + \rho_{\mathrm{Cu}} - \rho_{\mathrm{H_2O}}, \quad (3)$$

where $\rho_{n\mathrm{H_2O/Cu}}$, ρ_{Cu}, and $\rho_{n\mathrm{H_2O}}$ are the electron densities of the particular $n$$H_2O$/Cu(111) adsorption system under consideration, the isolated Cu(111) surface, and the isolated H_2O molecule(s) each in the exact structure they adopt in the adsorption system. Electron density difference plots such as this capture the rearrangement of the electron density upon making the adsorption bond and in this case demonstrate the key role played by the $1b_1$ orbital.

Moving to the H_2O dimer we show in Fig. 6(b) a similar electron density difference plot. From this is it is clear that the H bond donor interacts more strongly with the substrate than the acceptor does, which is what we would expect based on the structure alone. Further, it can be seen that the donor of the dimer interacts in a similar manner as the H_2O monomer does, *i.e.*, through the H_2O $1b_1$ orbital. Since the nature of the H bond in the adsorbed and gas phase dimers is similar (*cf.* Fig. 6(c)

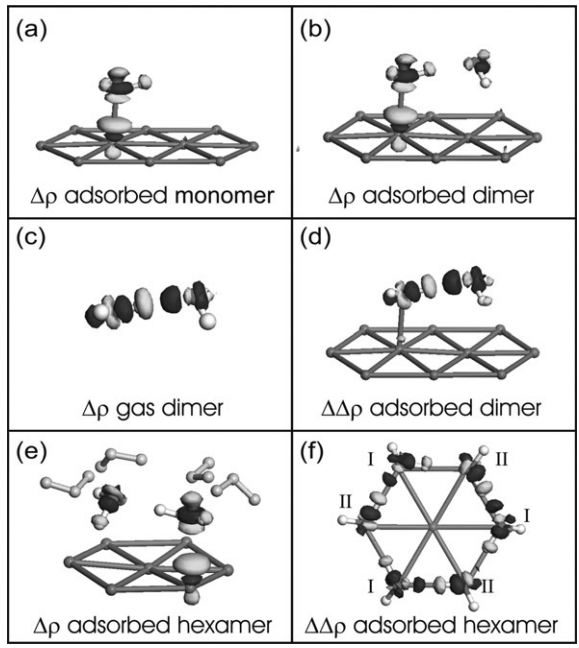

Fig. 6 Isosurfaces of constant electron density difference ($\Delta\rho$) and electron density "rearrangement" ($\Delta\Delta\rho$) as defined in eqn (3) and (4), respectively. $\Delta\rho$ is displayed for H_2O monomer adsorption (a), H_2O dimer adsorption (b), a gas phase H_2O dimer (c), and H_2O hexamer adsorption (e). $\Delta\Delta\rho$ is displayed for the adsorbed H_2O dimer (d) and the adsorbed H_2O hexamer (f). Dark isosurfaces correspond to regions of electron accumulation and light isosurfaces to regions of electron depletion. In (a), (b), (c), and (e) the units are 2×10^{-2} e Å^{-3}, and in (d) and (f) the units are 5×10^{-2} e Å^{-3}. For clarity in (e) $\Delta\rho$ is only displayed around the two front-most H_2O molecules and Cu atoms.

and (d)) it remains reasonable to seek insight into the nature of the adsorption bond by considering the electronic structure of the adsorbate in the gas phase, as we did for the H_2O monomer. Thus in Fig. 5(b) we display the energy level diagram for the high energy occupied orbitals of the gas phase H_2O dimer. Fig. 5(b) provides an immediate explanation for why the donor interacts more strongly with the substrate than the acceptor does and why this interaction is, like the monomer, mediated through the $1b_1$ orbital. Specifically, it can be seen that this is because the HOMO of the gas phase dimer is a $1b_1$-like orbital located on the H bond donor, and that this $1b_1$-like orbital remains a non-bonding orbital, not being involved in the H bond. On the other hand the $1b_1$-like orbital on the acceptor is not free being shifted to a lower energy through the formation of the H bond. Thus the $1b_1$-like orbital of the H bond acceptor of the dimer is, in a chemical sense, "saturated" through its participation in the H bond and less inclined to bond with the substrate than the H bond donor.

A similar reasoning explains the symmetry broken buckled structure of the adsorbed hexamer. Indeed the structure of the hexamer is best understood by considering it as being comprised of three weakly interacting dimers. Within the (equilibrium) buckled adsorption structure the two types of water molecules interact differently with the substrate, as revealed by the electron density difference plot in Fig. 6(e). Again the low-lying H_2O molecules in the adsorbed hexamer interact with the surface through their $1b_1$ molecular orbitals whereas the high-lying H_2O molecules do not. Since, as we have seen above, the $1b_1$ orbital of H_2O is also implicated when H_2O acts as a H bond acceptor, we can anticipate that the low-lying H_2O molecules are rendered poor H bond acceptors through their bonding with the substrate. Indeed this is precisely what we see in the structure of the adsorbed

hexamer with the longer (2.76 Å) H bonds being formed when the low-lying H_2O molecules act mainly as H bond acceptors, whereas the shorter (2.63 Å) H bonds form when the high-lying H_2O molecules act mainly as H bond acceptors. The two types of H bond in the adsorbed hexamer is clear not only from the atomic structure, but also in the electronic structure. To illustrate this we examine the electron density "rearrangement" ($\Delta\Delta\rho$) within the adsorbed hexamer. This is defined here as

$$\Delta\Delta\rho = \rho_{6H_2O/Cu} + \rho_{Cu} - \rho_{3H_2O\text{ - I}/Cu} - \rho_{3H_2O\text{ - II}/Cu}, \quad (4)$$

where $\rho_{6H_2O/Cu}$ and ρ_{Cu} are the electron densities of the hexamer/Cu(111) adsorption system and the clean Cu(111) slab, respectively. $\rho_{3H_2O\text{-I}/Cu}$ and $\rho_{3H_2O\text{-II}//Cu}$ are the electron densities of two subsets of the 6 adsorbed H_2O molecules, as labelled in Fig. 6(f). The two subsets of H_2O molecules are selected so that the quantity $\Delta\Delta\rho$ essentially reveals the H_2O–H_2O interaction in the adsorbed hexamer. Clearly from Fig. 6(f) it can be seen that the stronger H bonds form when the high-lying waters act mainly as the acceptors of the H bond, whereas the weaker H bonds form when the low-lying waters act mainly as acceptors. Essentially what the buckled structure of the hexamer tells us is that there is a competition between the ability of a H_2O molecule to form a 'strong' bond with the surface and its ability to act as a 'strong' H bond acceptor.

5. Conclusions

In conclusion the initial results of a DFT study of H_2O clustering on Cu(111) have been reported. Clusters with 2–6 H_2O molecules have been examined and for each cluster low energy adsorption structures reported. In addition, several novel concepts have been illustrated such as the fact that high energy gas phase isomers with fewer H bonds can be stabilized upon adsorption and that the nature of the competition between water–water bonding and water–metal bonding is more subtle than previously realised with a clear distinction having been identified between H_2O molecules that act either as H bond donors or as H bond acceptors.

Acknowledgements

This work was conducted as part of a EURYI scheme award. See www.esf.org/euryi. Matthias Scheffler is thanked for valuable discussions and for carefully reading this manuscript.

References

1 P. A. Thiel and T. E. Madey, *Surf. Sci. Rep.*, 1987, **7**, 211, and references therein.
2 M. A. Henderson, *Surf. Sci. Rep.*, 2002, **46**, 1, and references therein.
3 A. Verdaguer, G. M. Sacha, H. Bluhm and M. Salmeron, *Chem. Rev.*, 2006, **106**, 1478, and references therein.
4 H. Ogasawara, B. Brena, D. Nordlund, M. Nyberg, A. Pelmenschikov, L. G. M. Pettersson and A. Nilsson, *Phys. Rev. Lett.*, 2002, **89**, 276102.
5 S. Meng, L. F. Xu, E. G. Wang and S. W. Gao, *Phys. Rev. Lett.*, 2002, **89**, 176104.
6 C. Clay and A. Hodgson, *Curr. Opin. Solid State Mater. Sci.*, 2005, **9**, 11.
7 T. Schiros, S. Haq, H. Ogasawara, O. Takahashi, H. Ostrom, K. Andersson, L. G. M. Pettersson, A. Hodgson and A. Nilsson, *Chem. Phys. Lett.*, 2006, **429**, 415.
8 G. Zimbitas, S. Haq and A. Hodgson, *J. Chem. Phys.*, 2005, **123**, 174701.
9 C. Clay, S. Haq and A. Hodgson, *Chem. Phys. Lett.*, 2004, **388**, 39.
10 J. Cerdá, A. Michaelides, M. L. Bocquet, P. J. Feibelman, T. Mitsui, M. Rose, E. Fomin and M. Salmeron, *Phys. Rev. Lett.*, 2004, **93**, 116101.
11 T. Yamada, S. Tamamori, H. Okuyama and T. Aruga, *Phys. Rev. Lett.*, 2006, **96**, 036105.
12 A. Michaelides and P. Hu, *J. Am. Chem. Soc.*, 2001, **123**, 4235.
13 A. Michaelides and P. Hu, *J. Chem. Phys.*, 2001, **114**, 513.
14 G. Held, C. Clay, S. D. Barrett, S. Haq and A. Hodgson, *J. Chem. Phys.*, 2005, **123**, 064711.
15 P. J. Feibelman, *Science*, 2002, **295**, 99.

16 G. S. Karlberg, F. E. Olsson, M. Persson and G. Wahnstrom, *J. Chem. Phys.*, 2003, **119**, 4865.
17 A. Michaelides, A. Alavi and D. A. King, *J. Am. Chem. Soc.*, 2003, **125**, 2746.
18 C. Clay, S. Haq and A. Hodgson, *Phys. Rev. Lett.*, 2004, **92**, 046102.
19 G. A. Kimmel, N. G. Petrik, Z. Dohnatek and B. D. Kay, *Phys. Rev. Lett.*, 2005, **95**, 166102.
20 M. Nakamura and M. Ito, *Chem. Phys. Lett.*, 2004, **384**, 256.
21 M. Nakamura and M. Ito, *Chem. Phys. Lett.*, 2005, **404**, 346.
22 S. Yamamoto, A. Beniya, K. Mukai, Y. Yamashita and J. Yoshinobu, *J. Phys. Chem. B*, 2005, **109**, 5816.
23 K. Morgenstern and J. Nieminen, *Phys. Rev. Lett.*, 2002, **88**, 066102.
24 T. Mitsui, M. K. Rose, E. Fomin, D. F. Ogletree and M. Salmeron, *Science*, 2002, **297**, 1850.
25 K. Morgenstern and K.-H. Rieder, *J. Chem. Phys.*, 2002, **116**, 5746.
26 A. Michaelides, V. A. Ranea, P. L. de Andres and D. A. King, *Phys. Rev. Lett.*, 2003, **90**, 216102.
27 A. Michaelides, *Appl. Phys. A*, 2006, **85**, 415.
28 V. A. Ranea, A. Michaelides, R. Ramirez, P. L. de Andres, J. A. Verges and D. A. King, *Phys. Rev. Lett.*, 2004, **92**, 136104.
29 S. Meng, E. G. Wang and S. Gao, *Phys. Rev. B*, 2004, **69**, 195404.
30 S. Haq, C. Clay, G. R. Darling and A. Hodgson, *Phys. Rev. B*, 2006, **73**, 115414.
31 P. Vassilev, R. A. van Santen and M. T. M. Koper, *J. Chem. Phys.*, 2005, **122**, 054701.
32 V. A. Ranea, A. Michaelides, R. Ramirez, J. A. Verges, P. L. de Andres and D. A. King, *Phys. Rev. B*, 2004, **69**, 205411.
33 A. Michaelides, V. A. Ranea, P. L. de Andres and D. A. King, *Phys. Rev. B*, 2004, **69**, 075409.
34 D. Sebastiani and L. Delle Site, *J. Chem. Theory Comput.*, 2005, **1**, 78.
35 A. Michaelides and K. Morgenstern, (submitted).
36 A. Michaelides, A. Alavi and D. A. King, *Phys. Rev. B*, 2004, **69**, 113404.
37 M. D. Segall, P. J. D. Lindan, M. J. Probert, C. J. Pickard, P. J. Hasnip, S. J. Clark and M. C. Payne, *J. Phys.: Condens. Matter*, 2002, **14**, 2717.
38 D. Vanderbilt, *Phys. Rev. B*, 1990, **41**, R7892.
39 (*a*) J. P. Perdew, K. Burke and M. Ernzerhof, *Phys. Rev. Lett.*, 1996, **77**, 3865; (*b*) J. P. Perdew, K. Burke and M. Ernzerhof, *Phys. Rev. Lett.*, 1997, **78**, 1396.
40 *Handbook of Chemistry and Physics*, ed. D. R. Lide, CRC, London, 80th edn, 1999.
41 H. J. Monkhorst and J. D. Pack, *Phys. Rev. B*, 1976, **13**, 5188.
42 B. Hammer, L. N. Hansen and J. K. Nørskov, *Phys. Rev. B*, 1999, **59**, 7413.
43 C. Adamo and V. Barone, *J. Chem. Phys.*, 1999, **110**, 6158.
44 The calculations on the Cu clusters were performed with the Gaussian03 code, M. J. Frisch, G. W. Trucks, H. B. Schlegel, G. E. Scuseria, M. A. Robb, J. R. Cheeseman, J. A. Montgomery, Jr., T. Vreven, K. N. Kudin, J. C. Burant, J. M. Millam, S. S. Iyengar, J. Tomasi, V. Barone, B. Mennucci, M. Cossi, G. Scalmani, N. Rega, G. A. Petersson, H. Nakatsuji, M. Hada, M. Ehara, K. Toyota, R. Fukuda, J. Hasegawa, M. Ishida, T. Nakajima, Y. Honda, O. Kitao, H. Nakai, M. Klene, X. Li, J. E. Knox, H. P. Hratchian, J. B. Cross, V. Bakken, C. Adamo, J. Jaramillo, R. Gomperts, R. E. Stratmann, O. Yazyev, A. J. Austin, R. Cammi, C. Pomelli, J. Ochterski, P. Y. Ayala, K. Morokuma, G. A. Voth, P. Salvador, J. J. Dannenberg, V. G. Zakrzewski, S. Dapprich, A. D. Daniels, M. C. Strain, O. Farkas, D. K. Malick, A. D. Rabuck, K. Raghavachari, J. B. Foresman, J. V. Ortiz, Q. Cui, A. G. Baboul, S. Clifford, J. Cioslowski, B. B. Stefanov, G. Liu, A. Liashenko, P. Piskorz, I. Komaromi, R. L. Martin, D. J. Fox, T. Keith, M. A. Al-Laham, C. Y. Peng, A. Nanayakkara, M. Challacombe, P. M. W. Gill, B. G. Johnson, W. Chen, M. W. Wong, C. Gonzalez and J. A. Pople, *GAUSSIAN 03 (Revision C.02)*, Gaussian, Inc., Wallingford, CT, 2004.
45 S. Maheshwary, N. Patel, N. Sathyamurthy, A. D. Kulkarni and S. R. Gadre, *J. Phys. Chem. A*, 2001, **105**, 10525.